**Correspondence to:**
R. H. Ward,
rebecca.ward@bristol.ac.uk

**Author Contributions:**
**Conceptualization:** Rebecca H. Ward, Anita L. Ganesan
**Data curation:** Colm Sweeney, John B. Miller, Mathias Goeckede, Tuomas Laurila, Juha Hatakka, Viktor Ivakov, Motoki Sasakawa, Toshinobu Machida, Shinji Morimoto, Daisuke Goto
**Formal analysis:** Rebecca H. Ward

# Increasing Methane Emissions and Widespread Cold-Season Release From High-Arctic Regions Detected Through Atmospheric Measurements

Rebecca H. Ward[1] , Colm Sweeney[2] , John B. Miller[2] , Mathias Goeckede[3], Tuomas Laurila[4] , Juha Hatakka[4], Viktor Ivakov[5], Motoki Sasakawa[6] , Toshinobu Machida[6] , Shinji Morimoto[7] , Daisuke Goto[8] , and Anita L. Ganesan[1]

[1]School of Geographical Sciences, University of Bristol, Bristol, UK, [2]National Oceanic and Atmospheric Administration/Global Monitoring Laboratory, Boulder, CO, USA, [3]Max Planck Institute for Biogeochemistry, Jena, Germany, [4]Finnish Meteorological Institute, Helsinki, Finland, [5]Voeikov Main Geophysical Observatory, St Petersburg, Russia, [6]Center for Global Environmental Research, National Institute for Environmental Studies, Tsukuba/Ibaraki, Japan, [7]Tohoku University, Sendai, Japan, [8]National Institute of Polar Research, Tokyo, Japan

**Abstract**   Rising Arctic temperatures pose a threat to the large carbon stores trapped in Arctic permafrost. To assess methane emissions in high-Arctic regions, we analyzed atmospheric data from Alaska and Siberia using two methods: (a) a wind sector approach to calculate emission changes based on concentration enhancements using wind direction, and (b) an inversion method utilizing a high-resolution atmospheric transport model. Incorporating data after 2015, we observed a significant rise in methane emissions ($0.018 \pm 0.005$ Tg yr$^{-2}$ from 2000 to 2021) from Alaska's North Slope, indicating a shift from previous analyses. We find 34%–50% of yearly emissions occurred in the late season (September–December) consistently across multiple years and regions, which is historically underestimated in models and inventories. Our findings reveal significant changes occurring in the Arctic, highlighting the crucial role of long-term atmospheric measurements in monitoring the region, especially during the cold season.

**Plain Language Summary**   The Arctic is undergoing dramatic changes with temperatures increasing at four times the global average. This increase in temperature threatens to thaw the large stores of frozen carbon in Arctic soils which can be released as methane, a more potent greenhouse gas than carbon dioxide. We use measurements of methane in the atmosphere from four Arctic Ocean coastal stations to quantify emissions from the surface. We find that emissions from the North Slope of Alaska have been increasing over the past three decades, which reflects a change from previous analyses. Additionally, we show large and consistent emissions from September to December across multiple Arctic regions. This season has traditionally been underestimated in global methane budgets and providing accurate methane quantification is vital for climate change mitigation. Our results show that important change is occurring in the Arctic, and long-term atmospheric data can be used to monitor this change, particularly in the cold season.

## 1. Introduction

The Arctic is experiencing temperature increase four times higher than the global average (Rantanen et al., 2022), yet its role in the global carbon budget is poorly constrained (Meredith et al., 2019). With 1,100–1,500 Pg of carbon stored within the permafrost (Hugelius et al., 2014), rising temperatures could result in this carbon being released into the atmosphere as carbon dioxide and methane. In particular, release as methane could have a major impact on the global climate, due to the potency of methane as a greenhouse gas (Myhre et al., 2013). It is therefore crucial to understand and quantify terrestrial sources of methane in the Arctic, and to advance methods that offer long-term monitoring in the region.

Recent studies have shown that significant tundra emissions of methane may be occurring during the cold season (September–May), once temperatures have lowered and snow cover has returned (Arndt et al., 2019; Bao et al., 2021; Mastepanov et al., 2008, 2013; Treat et al., 2018; Zona et al., 2016). These cold season emissions are the result of a prolonged "zero-curtain", allowing the permafrost active layer to remain thawed whilst the ground above and below is frozen (Hinkel et al., 2001). Over 50% of the Arctic's annual methane emissions could be

**Investigation:** Rebecca H. Ward, Colm Sweeney, John B. Miller
**Methodology:** Rebecca H. Ward, Anita L. Ganesan
**Resources:** Colm Sweeney, John B. Miller, Mathias Goeckede, Tuomas Laurila, Juha Hatakka, Viktor Ivakov, Motoki Sasakawa, Toshinobu Machida, Shinji Morimoto, Daisuke Goto
**Software:** Rebecca H. Ward
**Supervision:** Anita L. Ganesan
**Validation:** Rebecca H. Ward
**Visualization:** Rebecca H. Ward
**Writing – original draft:** Rebecca H. Ward
**Writing – review & editing:** Rebecca H. Ward, Colm Sweeney, John B. Miller, Mathias Goeckede, Tuomas Laurila, Juha Hatakka, Viktor Ivakov, Motoki Sasakawa, Toshinobu Machida, Shinji Morimoto, Daisuke Goto, Anita L. Ganesan

originating from the cold season (Zona et al., 2016), a finding often overlooked in global emission assessments (Saunois et al., 2020).

The majority of high-Arctic zero-curtain studies have been conducted in Alaska (Arndt et al., 2019; Bao et al., 2021; Tao et al., 2021; Zona et al., 2016). The few studies made over Siberia also suggest the potential significance of the cold season on the annual methane budget (Kittler et al., 2017; Rößger et al., 2022). Most zero-curtain studies rely on flux measurements, which capture small spatial scales (hundreds of meters) and may not accurately reflect pan-Arctic scales.

A small number of atmospheric measurement stations situated across the Arctic coastline continuously measure atmospheric methane mole fraction. In contrast to flux measurements, well-calibrated atmospheric mole fraction measurements detect small changes in atmospheric composition that represent emissions over a large spatial scale (hundreds of kilometers). These measurements are made using instruments that often are in operation for years to decades, allowing the detection of gradual changes in emissions over time. Moreover, measuring fluxes during the cold season in the Arctic has historically posed challenges due to adverse weather conditions. Continuous and automated atmospheric measurements offer a means to monitor these periods with fewer logistical constraints.

Despite significant increases in surface air temperature over the past decades, Sweeney et al. (2016), showed that changes in July–September methane emissions from the North Slope of Alaska between 1986 and 2015 were not statistically different from zero. However, a significant trend in November–December emissions was observed. This study employed mole fraction measurements from the National Oceanic and Atmospheric Administration's Barrow Observatory in Utqiagvik, Alaska. Wind direction was used to identify the times that $CH_4$ mole fraction reflected a clean "background" sector (air coming from the ocean before arriving at Barrow), versus times that mole fractions represented land emissions (air passing over land). The difference between land and background mole fractions reflected the strength of emissions.

Emissions can also be inferred from atmospheric mole fractions through inverse modeling, which has the benefit over directly using mole fraction enhancements (as in Sweeney et al. (2016)), in that it takes into account more complex meteorological information such as changes in planetary boundary layer height and wind speed. Arctic methane emissions derived from inverse methods (Berchet et al., 2015; Ishizawa et al., 2019; Tenkanen et al., 2021; Thompson et al., 2017; Tsuruta et al., 2023; Wittig et al., 2023) have primarily focused on large-scale regions, such as entire countries or highly inundated regions such as the West Siberian Lowlands or Hudson Bay Lowlands. Additionally, these studies have not focused on late-season emissions from the high Arctic, a region that contains a large proportion of dry tundra (less than 20% inundation), which has the potential to emit significantly during the cold season (Treat et al., 2018; Zona et al., 2016). Zona et al. (2016) found that tundra with less than 5% inundation was strongly emitting during the cold season.

Our study uses multiple methods to quantify emissions over three high-latitude Arctic tundra regions—the North Slope of Alaska, the Taymyr Peninsula and the East Siberian Lowlands. These regions were selected because they are in the rapidly warming high Arctic (Rantanen et al., 2022; Turetsky et al., 2019), and contain large stores of carbon (Hugelius et al., 2014). The defined regions also contain a high proportion of dry tundra (Olefeldt et al., 2021), which are much less inundated than more monitored regions such as the Hudson Bay Lowlands and West Siberian Lowlands. We determine whether late season emissions are prevalent across the three regions and are persistent over time, and whether emissions are exhibiting significant changes over decadal timescales.

## 2. Methods

We employ two approaches to determine trends and to quantify emissions. The first method extends the results of Sweeney et al. (2016), including data from 2016 to 2021 in order to assess any changes North Slope emission trends. As this method is based on calculating enhancements in methane mole fraction from the land versus background sectors, it is only able to determine relative changes in emissions over time. The second method uses a hierarchical Bayesian inversion framework, with an atmospheric transport model (Numerical Atmospheric-dispersion Modeling Environment (NAME) (Jones et al., 2007)). The atmospheric transport model provides a pathway for directly estimating emissions from mole fractions by simulating the dilution of emissions in the atmosphere, and thus offers absolute quantification of emissions. Model meteorological fields used to run NAME are available from the year 2000 and emissions are quantified from 2000 to 2021 for the North Slope and from
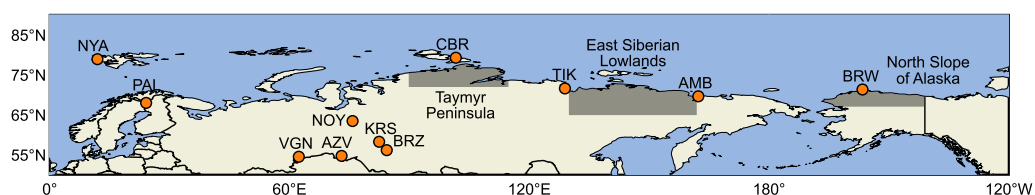
**Figure 1.** Location of the atmospheric measurement stations and three high-latitude regions in this study—the Taymyr Peninsula, the East Siberian Lowlands and the North Slope of Alaska.

2014 to 2021 for the two Siberian regions. Emissions derived through the inversion are masked for anthropogenic emissions using filters and sector attribution methods.

Throughout this work, we define the early (April–June), summertime (July–August) and late (September–December) seasons to correspond to typical spring thaw, growing season and fall zero curtain periods (Zona et al., 2016) for the high Arctic.

### 2.1. Measurements

We used high frequency in situ atmospheric mole fraction measurements of $CH_4$ from 11 sites across the Arctic (described in Table S1 in Supporting Information S1, locations shown in Figure 1). In North America, we used the continuous record from the NOAA Observatory in Barrow (BRW) (Lan et al., 2022) from 1986 to 2021. We used measurements three coastal Siberian sites, Ambarchik (AMB) (Reum et al., 2019), Cape Baranova (CBR) and Tiksi (TIK) (Laurila et al., 2017). Measurements at AMB were made by the Max Planck Institute for Biogeo-chemistry (MPI-BGC). Measurements at CBR (2015–2020) and TIK (2013–2020) are both part of the Finnish Meteorological Institute (FMI) network. In the West Siberian Lowlands we used 5 Japan–Russia Siberian Tall Tower Inland Observation Network (JR-STATION) sites from the National Institute for Environmental Studies (NIES)—Azovo (AZV), Berezorechka (BRZ), Karasevoe (KRS), Noyabrsk (NOY) and Vaganovo (VGN) (Sasakawa et al., 2010). These sites were reported on the NIES-94 scale and converted to the WMOX2004A scale for this work. There are multiple inlets used for each site, in each case we use the measurements from the highest inlet. In Europe we used the FMI site Pallas, Finland (PAL) (Laurila et al., 2017), and the National Institute of Polar Research (NIPR) site Ny-Ålesund, Svalbard (NYA) (Morimoto et al., 2017).

### 2.2. Wind Sector Analysis at Barrow

This analysis was closely modeled on the framework established by Sweeney et al. (2016), adhering as closely as possible to their original design. To do this we developed new analysis code, incorporating guidance directly from the authors, to replicate the procedures outlined in their manuscript. Each hourly averaged $CH_4$ measurement in the data set was categorized by wind direction into sectors. The background sector was 0–90°, considered to be representative of well-mixed background air. The "land" sector at 150°–210°, is a region of predominately Arctic soils and lakes. The remaining regions were included anthropogenic emissions, with Utqiagvik (210°–360°) and Prudhoe Bay fossil fuel extraction field (90°–150°) in close proximity. The measurements were further filtered for times when the standard deviation within the hour was <10 ppb, and the wind speed was <3.0 ms$^{-1}$, to avoid analysis of stagnant air. Background measurements were averaged monthly and smoothed using a harmonic fitting routine described in Thoning et al. (1989) (Figure S1 in Supporting Information S1). Enhancements in $CH_4$ mole fraction were calculated as mole fractions from the land sector minus mole fractions from the background sector. Trends in enhancements were studied for different three time periods across the year, to quantify seasonal land sector emissions and investigate the presence of zero curtain emissions. Calculation of uncertainties in trends are described in Text S1 in Supporting Information S1.

### 2.3. Inversion Method

To calculate emissions estimates from the atmospheric mole fraction data, we first calculate a prior modeled mole fraction estimate using sensitivity maps derived from the UK Met Office NAME model and a priori flux fields. Arctic wide a priori flux fields were produced using bottom-up emissions inventories of terrestrial sources, anthropogenic sources and fires. Further details of the prior emissions are shown in Tables S2 and S3 in

Supporting Information S1, along with prior (Figure S2 in Supporting Information S1). We calculate a posterior distribution of emissions using a hierarchical Bayesian Markov Chain Monte Carlo inversion framework.

The model representation of $y$, a vector containing $CH_4$ mole fractions, is defined in Equation 1 as:

$$y = \mathbf{H}x + \epsilon \tag{1}$$

where $\mathbf{H}$ is a sensitivity matrix, describing the relationship between atmospheric mole fractions and emissions from the surface, $x$ contains the emissions and $\epsilon$ contains the model-measurement errors. $\mathbf{H}$ is the product of sensitivity maps that are produced using an atmospheric transport model, and a priori flux fields.

We solved for $x$ using a hierarchical Bayesian inversion framework (Equation 2). This method is described in Ganesan et al. (2014) and Say et al. (2020). To avoid using subjective uncertainties chosen by judgment, we included additional "hyper-parameters", represented by $\theta$.

$$p(x, \theta | y) \propto p(y | x, \theta) p(x | \theta) p(\theta) \tag{2}$$

These hyper-parameters describe the unknown model-measurement uncertainties as additional probability density functions (PDFs) that are then propagated in the inversion. Thus, the derived emissions and their uncertainties account for this additional level of model uncertainty.

There is no analytical solution to solve for a posterior optimization of $x$, so a sampling technique is required. We used Markov Chain Monte Carlo (MCMC) with No U-Turn Sampler described in Say et al. (2020). MCMC also allows for the use of non-Gaussian PDFs to describe each parameter.

Hourly model sensitivity maps or footprints were produced to provide the quantitative relationship between the hourly averaged measured mole fractions at each site and the surface emissions. Footprints were calculated using the Met Office's NAME, a Lagrangian Particle Dispersion Model (Jones et al., 2007). This model tracks particles released from the measurement site backwards in time using meteorological data from a numerical weather prediction model, the Met Office's Unified Model (UM). Particles were tracked for up to 30 days, or when they have left the regional domain. Recording the exit times and locations provides the sensitivity of measured mole fractions to the boundary conditions of the regional domain. Our footprints were spatially resolved on a $0.234° \times 0.352°$ grid across the whole Arctic domain. A model time step of 1 min was chosen to prevent grid cells from being skipped during a time step due to the small size of grid cells near the poles. Southward of 80°N, it is not expected that model grid cells will be skipped within the 1 min time step. The Arctic domain used here spans 36° to 90°N and all longitudes. This zonal coverage was chosen to include the impacts of sources that could traverse the Arctic within the model simulation. Average model-measurement sensitivity maps for each inversion are shown in Figure S3 in Supporting Information S1.

A quadtree algorithm was used to aggregate grid cells so that 100 emission parameters were solved for in the inversion. Higher resolution regions are estimated near the sites and coarser resolution regions farther away, where the measurements have lower sensitivity. The model solved for the scaling of the prior in each of these regions. These basis functions were produced for the BRW inversion and the AMB-CBR-TIK inversion separately as shown in Figure S4 in Supporting Information S1. The emissions scaling factors had a prior PDF that is Gaussian, truncated at zero to prevent non-physical negative emissions. These scaling factor PDFs were given a mean of 1 and a standard deviation of 2.

Due to the footprints extending across all latitudes, there is only one boundary at the southern boundary. For the Siberian inversions, mole fraction curtains at the boundary of the domain were determined by the global methane model CAMS v19r1 (Inness et al., 2019). This product runs until 2019, so for subsequent years the background was assumed to be the same as that of 2019. A scaling parameter for the Southern boundary condition is included in the inversion with a PDF that is Gaussian, truncated at 0, with a mean of 1 and a standard deviation of 0.02 (corresponding approximately to 40 ppb), thus the background is optimized during the inversion alongside the emissions and model-measurement error.

For the BRW inversions, we subtracted a smoothed background (as described in the wind sector method, see main paper methods) from the raw data, so our results from the wind sector and inversions used consistent approaches. This smoothed background is shown in Figure S1 in Supporting Information S1. This background only fits the

data well for the April–December months, so January–March months were not included in the inversion. We also carried out a sensitivity test for the BRW inversion using the CAMS background (same method as the Siberian inversion), which can be seen in Figure S5 in Supporting Information S1.

The uncertainty in observations is a combination of model and measurement uncertainty. Measurement uncertainty was included as the uncertainty directly taken from each hourly measurement. The model uncertainty was a hyper-parameter with a uniform PDF between 0.5 and 30 ppb. The model and measurement uncertainties were combined in quadrature to result in the overall uncertainty applied to each data point.

We filtered out data that is influenced by local emissions, which cannot be not resolved in the inversion. At BRW, the first filter was wind direction. With the town of Utqiagvik located to the West, times when the measured wind direction is 210°–360° are removed because of the potential influence of anthropogenic emissions from the town. The second filter was to remove times when measured wind speeds were less than 3 m/s to avoid stagnant conditions. For the other sites, we did not use measured wind direction and speeds because there was no clear pattern of wind directions being heavily influenced by anthropogenic emissions. We instead used a "local influence filter". The local influence filter uses a similar method to Lunt et al., 2021; Lunt et al., 2021), whereby if the 25 grid cells surrounding the site contributed to greater than 10% of the total NAME footprint for that time, the measurement is filtered. The same local influence filter at Barrow was also used as a sensitivity study (see Figure S6 in Supporting Information S1), which showed no difference to the wind speed/direction filter.

We partitioned our posterior emissions using the fraction of the natural, anthropogenic and fire emissions in each grid cell of our prior, similarly to Tunnicliffe et al. (2020). In the study regions, the types of source are largely separated spatially as shown in Figure S7 in Supporting Information S1.

The performance of each inversion performance is characterized in Figure S8 in Supporting Information S1 for the North Slope inversion and Figure S9 in Supporting Information S1 for the Siberia inversion.

## 3. Results and Discussion

### 3.1. $CH_4$ Emissions and Trends From the North Slope of Alaska

While Sweeney et al. (2016) previously showed no significant increase in summertime $CH_4$ enhancements, we show by extending the observational record through 2021, that a statistically significant trend can now be detected across July–August. We report a wind sector trend of $0.87 \pm 0.40$ ppb/yr in summertime $CH_4$ enhancements from the North Slope of Alaska over the period 1986–2021 (Figure 2a). The wind sector trend over the period 2000–2021 is $2.32 \pm 0.76$ ppb/yr. Using the inversion method, this 2000–2021 trend corresponds to a growth of $0.018 \pm 0.005$ Tg yr$^{-2}$. Average summertime inversion emissions increased from $0.50 \pm 0.09$ Tg/yr during 2000–2010 to $0.90 \pm 0.14$ Tg/yr during 2010–2021. Both methods suggest that summertime emissions from the North Slope have increased between 90% and 100% over the last 20 years.

Our results also confirm that the late season (September–December) trend first shown by Sweeney et al. (2016) has persisted through to 2021. We find a wind-sector trend of $0.36 \pm 0.34$ ppb/yr from 1986 to 2021, and a wind-sector trend of $0.87 \pm 0.71$ ppb/yr from 2000 to 2021, which corresponds an inversion trend of $0.017 \pm 0.003$ Tg yr$^{-2}$. We find a small positive trend in wind-sector enhancements in the early season for the 1986–2021 and 2000–2021, however this is not reflected with our inversion method. We suspect that this uncertain trend is largely driven by emissions from June, a month representing mixed conditions.

Comparisons with previous inversion studies over the North Slope are challenging due to their reliance on short-term campaigns or quantification over all of North America. However, Miller et al. (2016) found North Slope emissions of $1.74 \pm 0.44$ Tg/yr May–October using measurements from the CARVE missions across 2012–2014. We find lower emissions with our inversion method of $0.70 \pm 0.09$ Tg/yr for the 2012–2014 mean.

Given the Arctic's rapid warming over the last few decades, we investigated temperature trends over the North Slope. We find significant positive trends in air temperature anomaly, across the early and late seasons (Figure 3a). Anomalies (temperatures relative to the 1986–2021 mean) were calculated by taking the temperatures when winds were coming from the land sector and subtracting the mean monthly background temperature as per the wind sector method. Every 10 years at Barrow, the air temperature increases by 1.6° in the September–December time frame and 1.0° in the April–June time frame. We extend the method of Sweeney et al. (2016) to examine the temperature sensitivity of tundra methane emissions.
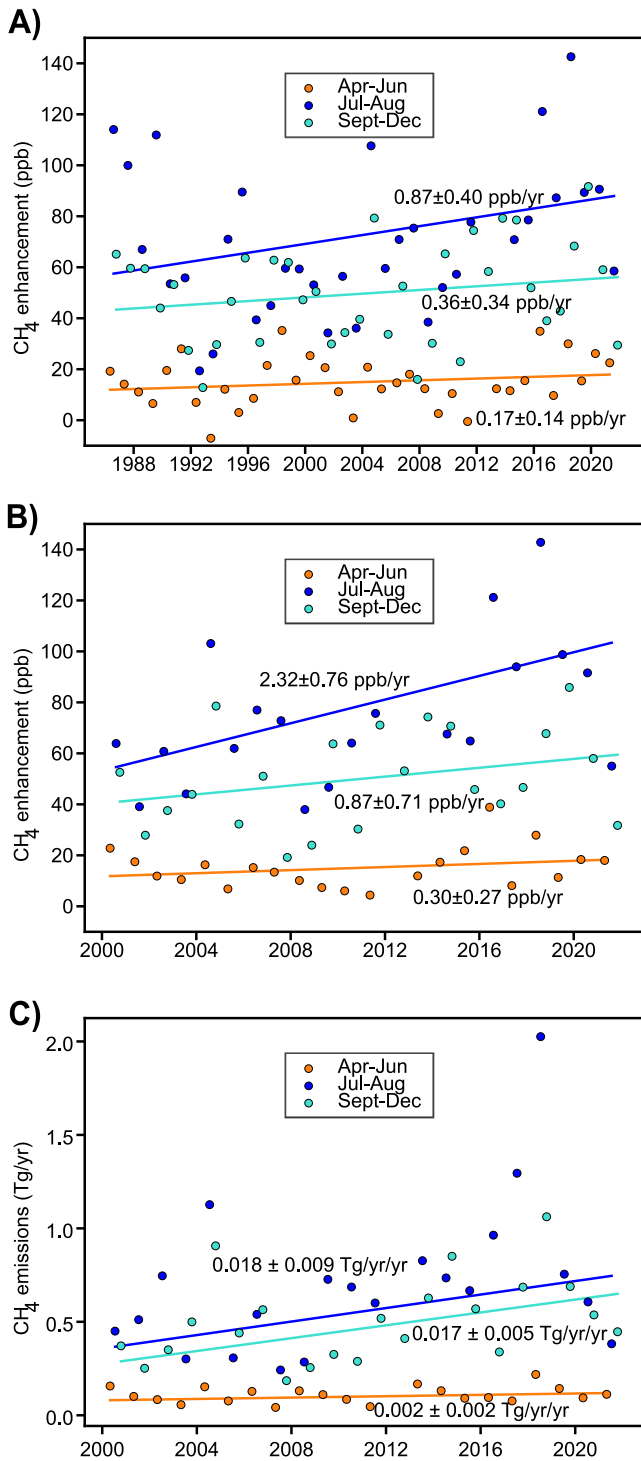
**Figure 2.** Trends in methane from the North Slope of Alaska. (a) $CH_4$ enhancements in ppb over the period 1986–2021. (b) Same as A but over 2000–2021. (c) Emissions in Tg/yr over 2000–2021. Uncertainties in the wind sector and inversion trends are found using a sampling method described in Text S1 in Supporting Information S1.

We find an air temperature sensitivity for the July–August time period of $5.3 \pm 2.6$ ppb/degree C (Figure 3b). This corresponds to a $Q_{10}$ value of 2.1, consistent with the findings of Sweeney et al. (2016). $Q_{10}$ is a parameter used in wetland models to estimate methane fluxes, indicating how methane production would change with a 10° temperature rise (Bloom et al., 2017; Xu et al., 2016). Our empirically-derived $Q_{10}$ value ($Q_{10} = \frac{[\Delta CH_4]_{T2}}{[\Delta CH_4]_{T1}}^{\frac{10}{T2-T1}}$.) sits within the middle of values used in the WetCHARTs full ensemble, which employs $Q_{10}$ values between 1 and 3 (Bloom et al., 2017).

Outside of summer months, air temperature is not a reliable predictor of emissions due to the insulating effect of snow (Arndt et al., 2019). Unfortunately, long-term soil temperature data sets are not available to evaluate the temperature sensitivity during the late season.

This new summertime trend challenges the idea that methane trends in the Arctic may be too small for detection by atmospheric measurements (Euskirchen et al., 2022). It not only marks a significant shift in this specific region but also may have broader implications for the pan-Arctic region given increasing Arctic temperatures (Rantanen et al., 2022), and the temperature sensitivity of emissions from the region over this time period (Figure 3b). The North Slope of Alaska is one of many biomes of the Arctic. Given the Arctic's diverse land and vegetation types (Olefeldt et al., 2021), trends the North Slope of Alaska might not represent the whole of the Arctic's complexity. Therefore, it highlights the importance of maintaining and expanding long-term measurement campaigns throughout the Arctic.

### 3.2. CH$_4$ Emissions From Siberia

We also quantify tundra emissions from two Siberian regions—the Taymyr Peninsula and East Siberian Lowlands—from late 2014 to 2021 (Figures 4a and 4b respectively). For the Siberian locations we used data from all 11 measurement sites shown in 1. The three coastal Siberian sites, Ambarchik (AMB), Tiksi (TIK) and Cape Baranova (CBR), have high sensitivity to our Siberian regions. Unlike Barrow Observatory measurements, which began in 1986, measurements from these stations only began in 2014 for AMB, 2015 for CBR and 2010 for TIK. As emissions are only quantified from late 2014, no trend analysis was performed.

We find average annual emissions from Arctic tundra in each region to be $0.47 \pm 0.07$ and $2.39 \pm 0.19$ Tg/yr for the Taymyr Peninsula and East Siberian Lowlands, respectively. Within these annual emissions we find summertime emissions of $0.12 \pm 0.03$ and $5.65 \pm 0.4$ Tg/yr and late season emissions of $0.63 \pm 0.09$ and $2.51 \pm 0.19$ Tg/yr for the Taymyr Peninsula and East Siberian Lowlands, respectively. Total emissions and emissions normalized by area for all three regions can be found in Table S5 in Supporting Information S1, and posterior emissions maps can be seen in Figure S10 in Supporting Information S1.

Our study was designed to investigate the three high-latitude Arctic regions at high spatial resolution and to perform in depth analyses on these smaller regions. We thus use observations from 11 stations that are sensitive to the target regions. We do not focus on the entire pan-Arctic region or North America, Canada, and Siberia to save computational cost.

Previous inversion studies over Siberia have mainly focused on larger regions (Thompson et al., 2017; Tsuruta et al., 2023; Wittig et al., 2023), for the purpose of pan-Arctic quantification, and therefore do not focus
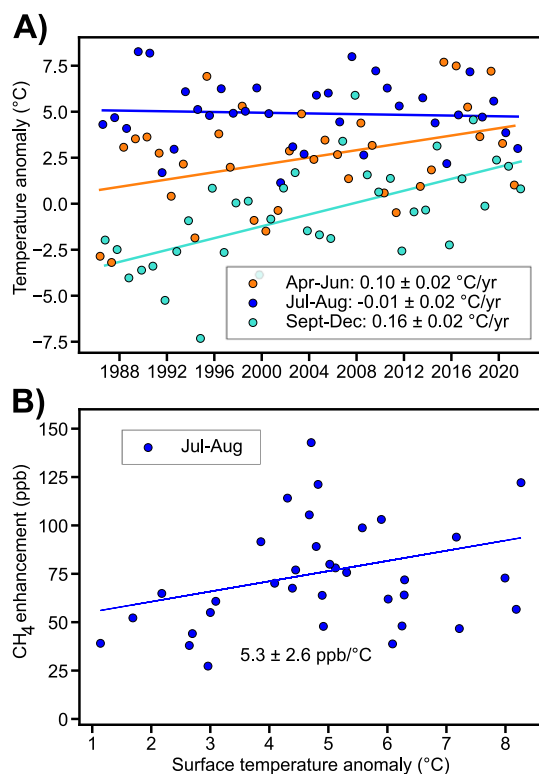
**Figure 3.** (a) Trends in surface temperature anomalies from Barrow (BRW) across April–June, July–August and September–December. (b) Surface temperature anomalies versus CH$_4$ enhancements for July–August at Barrow (BRW).

specifically on high latitude dry tundra regions. Other previous studies have also focused on boreal wetland regions such as the Hudson Bay Lowlands or West Siberian Lowlands (Thompson et al., 2017), which exhibit very different soil methane dynamics to our high-Arctic dry tundra regions. Consequently, these studies do not provide directly comparable results for our East Siberian Lowlands and Taymyr Peninsula regions. While Berchet et al. (2015) reported wetland emissions of 1–13 Tg/yr from a smaller Siberian lowlands region that overlapped a portion of our Taymyr Peninsula region, it also included emissions from the West Siberian Lowlands, an area with a variety of complex natural and anthropogenic emission sources.

### 3.3. Seasonal Cycles Across Three Arctic Regions

For each of the regions studied in the inversion, we infer strong emissions from the late season (Figure 5). We tested the impact of prior emissions on these results by deriving emissions using alternate priors with varying seasonal profiles.

All priors used the Emissions Database for Global Atmospheric Research (EDGAR) (Crippa et al., 2020) for anthropogenic emissions, and the Global Fire Emissions Database (GFED) (Randerson et al., 2017) for emissions from fires. The magnitude of the annual wetland emissions in all cases was the Global Methane Budget top-down 30°–90°N emissions of 46 Tg yr$^{-1}$(Saunois et al., 2020). We carried out an inversion that included oceanic emissions using (Weber et al., 2019), and found that using these emissions had a minimal impact on the estimation of wetland emissions, thus we opted not to include ocean emissions into our priors. The difference between the three priors lies in the seasonal and spatial distributions, which are shown in Figure 5a and Figure S3 in Supporting Information S1.

The "WetCHARTs" prior has a seasonal profile derived from the mean of the WetCHARTs extended ensemble (Bloom et al., 2017). Emissions peak in July, are low in the late shoulder season and are almost zero for the winter and early Spring. This profile is typical of most Arctic wetland models. The spatial distribution of this prior is the monthly inter-annually varying fractional wetland satellite product SWAMPs (Surface WAter Microwave Product Series) (Jensen & Mcdonald, 2019) over the years 2000–2019 (for 2020–2021 the spatial distribution is assumed to be that of 2019).

The "Late-season Zona" prior has a seasonal profile that extends further into the late shoulder season, based on Zona et al. (2016), and the spatial distribution of emissions was set in all months to the July value of SWAMPs. As shown in Zona et al. (2016), late season emissions from the North Slope of Alaska come from less inundated areas, and by setting the spatial distribution to that of a summertime month, we increase the potentially emitting area for our inversions in the late and early seasons. This profile is not represented in most wetland emission products, which base spatial distribution on inundation only.
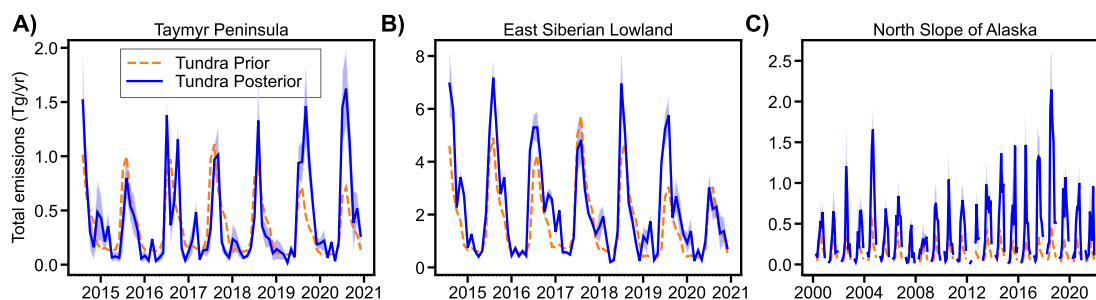


**Figure 4.** Methane emissions in Tg/yr from three high-Arctic regions. (a) The Taymyr Peninsula, (b) the East Siberian Lowlands and (c) the North Slope of Alaska.
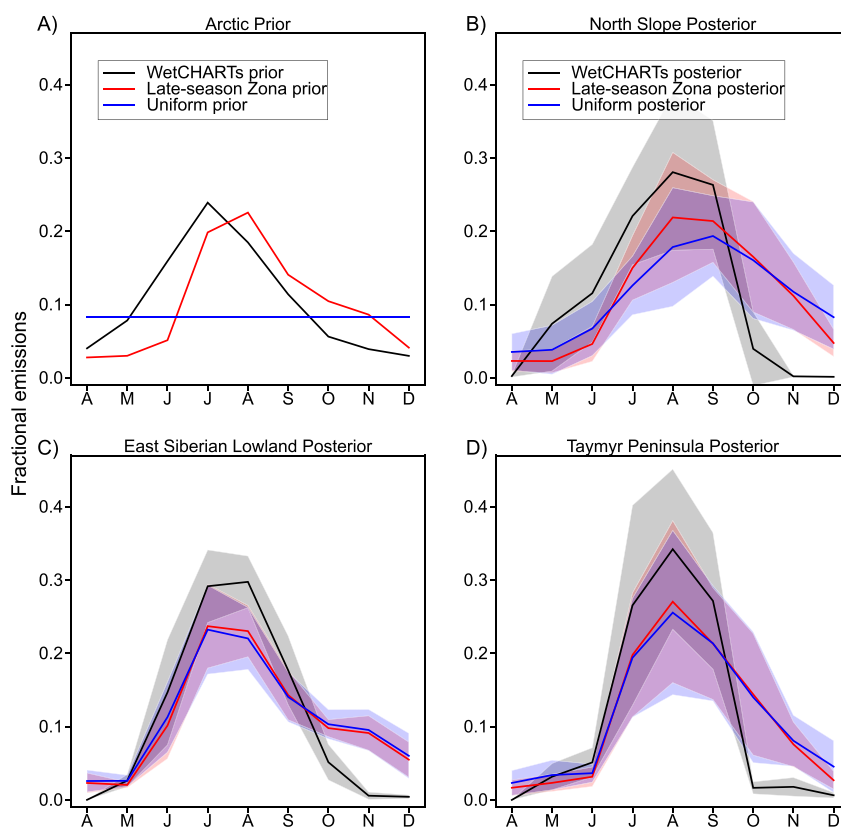
**Figure 5.** Average seasonal profiles (April–Deceber) as fraction of total annual emissions for the inverse estimates derived using different prior emissions. (a) The average prior over the three regions. (b–d) Posterior profiles for, (b) the North Slope. (c) East Siberian Lowlands and, (d) Taymyr Peninsula.

The "Uniform" prior distributes emissions evenly across each month and uses the same spatial distribution as the "Late-season Zona" prior.

Emissions derived using the three priors are shown in Figure 5a. The posterior seasonal cycle from the inversions using the "WetCHARTs" prior are restricted by the near zero emissions values of the prior in the late season. We see that with the "Late-season Zona" prior, the atmospheric data derives larger emissions much later in the season, and even with the completely "Uniform" prior, this emissions seasonal profile is preserved. The profile shapes are similar across all Arctic regions, indicating the presence of late season emissions when inversions are allowed to attribute emissions to these months. For the "Late-season Zona" prior, we find that on average, around 50% of annual emissions from the North Slope come from the late season, in agreement with Zona et al. (2016).

Tenkanen et al. (2021), conducted an inversion study using the remote sensing product Soil Moisture and Ocean Salinity Freeze/Thaw (SMOS F/T) (Rautiainen et al., 2016) to capture seasonal emissions from the cold season. They modified fluxes from the LPX-Bern DYPTOP model and assigned a low emission rate to the $1° \times 1°$ grid cells that are at least 90% frozen. Over the high latitude regions, including the North Slope of Alaska, the Taymyr Peninsula, and the East Siberian Lowlands, this model results in an overall decrease in emissions between Octobar–December from the standard model, resulting in a profile very similar to the WetCHARTS prior. Methane can still be released after the surface is frozen due to the zero curtain. As the SMOS F/T product is a surface-only product and not sensitive to the sub-surface conditions, this inversion may be underestimating key emissions from the zero curtain period.

Rößger et al. (2022) attribute 39% of emissions from the North Siberian Lena River Delta to be from the cold season. We find around 34% of emissions from East Siberian Lowland to be from the late season alone, and around 40% of emissions from the Taymyr Peninsula. These results show consistency in the prevalence of these late season emissions across three high Arctic regions. Our defined region for the East Siberian Lowland contains
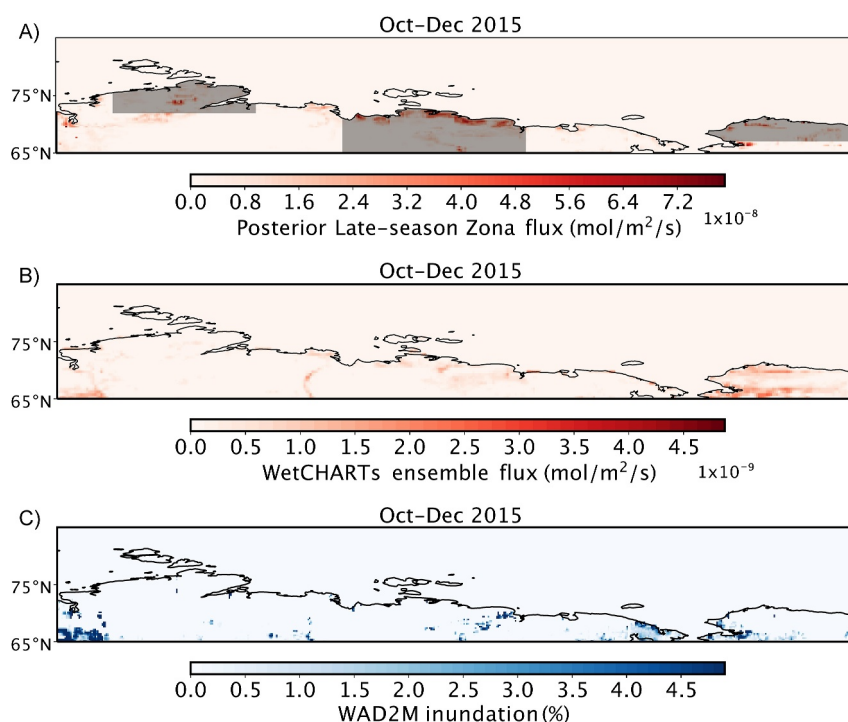
**Figure 6.** Flux and inundation averages for October–December 2015 for (a) the Posterior Late-season Zona flux derived in this study, (b) the WetCHARTs extended ensemble flux (Bloom et al., 2017) and (c) Wetland Area and Dynamics for Methane Modeling (WAD2M) inundation (Zhang et al., 2020). Regions shown in gray on panel (a) from left to right the Taymyr Peninsula, East Siberian Lowlands and North Slope of Alaska. Note the order of magnitude smaller scale between the Late-season Zona posterior flux and the WetCHARTs extended ensemble flux.

less dry tundra (43.6%) than the Taymyr Peninsula (69.7%) and North Slope of Alaska (63.0%) (Table S6 in Supporting Information S1. (Olefeldt et al., 2021), which could potentially explain the lower percentage of late season emissions we see from this region, given that late season emissions have been shown to be most significant in lowly inundated tundra (Zona et al., 2016).

The early season of April–June does not show strong emissions with any of the priors. Bao et al. (2021) found a much stronger methane emissions in the late shoulder season compared to the early shoulder season across three sites on the North Slope of Alaska. For the late season, a gradual freezing from both below and above the active layer prevents gas diffusion and therefore reduces $CH_4$ oxidation, and forces resultant $CH_4$ through cracks in the surface or plants. In the early season, surface-down thawing releases the remaining $CH_4$ gradually, which allows gas diffusion and ice melt to better oxidize the $CH_4$.

### 3.4. Comparison to Wetland Models

Whilst recent studies have found that wetland emissions could be overestimated due to the double counting of wetland extent resulting from the conflation of wetlands and small lakes (Thornton et al., 2016), it has also been suggested that emissions from drier areas, especially during the late season, may be overlooked (Zona et al., 2016). This land type is not detected by satellites as inundated, which is typically used as the basis for mapping $CH_4$ emissions in flux models (Bohn et al., 2015). Additionally, some areas may appear "dry" on an inundation map because the surface is frozen, even though emissions are still occurring from the sub-surface due to the zero curtain effect.

The WetCHARTs extended ensemble is an aggregation of models with two different inventory based spatial extents, either the Global Wetlands and Lakes Data set (GLWD) (Lehner & Döll, 2004) or ESA's GLOBCOVER wetland and freshwater land cover map (Bontemps et al., 2011), both combined with ERA Interim precipitation to define the temporal variability. The WetCHARTS models produce very low emissions in the late season

(Figure 6b) and the resulting seasonal profile restricts late-season emissions from being derived in inversions, as shown in Figure 5.

Recently, the Wetland Area and Dynamics for Methane Modeling (WAD2M) (Zhang et al., 2020) inundation data set was developed, which uses the satellite data set Surface WAter Microwave Product Series (SWAMPs), but includes the Northern Circumpolar Soil Carbon Database (NCSCD) (Hugelius et al., 2013) and the CircumArctic Wetlands based on Advanced Aperture Radar (CAWASAR) (Wilkman et al., 2018) inventories to capture under-represented wetland areas. While WAD2M extends the emitting area in the high-latitude regions in the summer months, Figure 6c shows that WAD2M inundation does not capture emitting areas in the late season.

From the work in this study, and in studies such as Zona et al. (2016), we have seen higher emissions from October to December compared to existing models. If future fluxes are based on inundation maps, emissions from areas in the high latitude Arctic in the late season will not be included. We suggest that future flux models make spatial extent adjustments based on low inundation areas in the late season and frozen ground that is still emitting due to the zero curtain effect.

## 4. Conclusions

We present estimates of methane emissions from three high-Arctic regions in Alaska and Siberia. We show that growing summertime methane emissions from the North Slope of Alaska can now be detected for the first time since the observational record at Barrow Observatory began in 1986. We show that summertime and late season emissions from the North Slope have increased by approximately 50% and 30%, respectively, over the past three decades. This study also shows that strong late season emissions (34%–50% of annual emissions) are persistent across the three high-latitude Arctic regions. These late season emissions indicate a widespread "zero curtain" effect on a pan-Arctic scale, particularly in dry tundra environments, emissions from which are not included in wetland assessments of emissions due to these land classes not appearing as inundated from satellite observations. These results suggest that wetland models should be modified to increase the emitting areas of high Arctic tundra in the late season and included in global assessments of methane emissions.

## Data Availability Statement

Inversion results for each region can be found at https://doi.org/10.5281/zenodo.10782558 (Ward, 2024a). Code and data the wind sector analysis results can be found at https://doi.org/10.5281/zenodo.10814752 (Ward, 2024b). Data for each site can be found as follows: BRW from NOAA GML (Schuldt et al., 2023). AMB from Edmond—the Open Research Data Repository of the Max Planck Society (Göckede et al., 2023). CBR from FMI (Laurila, 2023). TIK at the WDCGG (Ivakov et al., 2019). PAL from ICOS Carbon Portal (Hatakka & ICOS RI, 2022). NYA from NIPR (Morimoto & Goto, 2019). JR-STATION sites available at the Global Environmental Database —AZV (Sasakawa, 2023d), BRZ (Sasakawa, 2023b), KRS (Sasakawa, 2023e), NOY (Sasakawa, 2023a) and VGN (Sasakawa, 2023c).

## References

Arndt, K. A., Oechel, W. C., Goodrich, J. P., Bailey, B. A., Kalhori, A., Hashemi, J., et al. (2019). Sensitivity of methane emissions to later soil freezing in arctic tundra ecosystems. *Journal of Geophysical Research: Biogeosciences*, *124*(8), 2595–2609. https://doi.org/10.1029/2019JG005242

Bao, T., Xu, X., Jia, G., Billesbach, D. P., & Sullivan, R. C. (2021). Much stronger tundra methane emissions during autumn freeze than spring thaw. *Global Change Biology*, *27*(2), 376–387. https://doi.org/10.1111/gcb.15421

Berchet, A., Pison, I., Chevallier, F., Paris, J.-D., Bousquet, P., Bonne, J.-L., et al. (2015). Natural and anthropogenic methane fluxes in Eurasia: A mesoscale quantification by generalized atmospheric inversion. *Biogeosciences*, *12*(18), 5393–5414. https://doi.org/10.5194/bg-12-5393-2015

Bloom, A. A., Bowman, K. W., Lee, M., Turner, A. J., Schroeder, R., Worden, J. R., et al. (2017). A global wetland methane emissions and uncertainty dataset for atmospheric chemical transport models (WetCHARTs version 1.0). *Geoscientific Model Development*, *10*(6), 2141–2156. https://doi.org/10.5194/gmd-10-2141-2017

Bohn, T. J., Melton, J. R., Ito, A., Kleinen, T., Spahni, R., Stocker, B. D., et al. (2015). WETCHIMP-WSL: Intercomparison of wetland methane emissions models over west Siberia. *Biogeosciences*, *12*(11), 3321–3349. https://doi.org/10.5194/bg-12-3321-2015

Bontemps, S., Herold, M., Kooistra, L., Van Groenestijn, A., Hartley, A., Arino, O., et al. (2011). Revisiting land cover observations to address the needs of the climate modelling community. *Biogeosciences*, *9*(6), 2145–2157. https://doi.org/10.5194/bgd-8-7713-2011

Crippa, M., Solazzo, E., Huang, G., Guizzardi, D., Koffi, E., Muntean, M., et al. (2020). High resolution temporal profiles in the emissions database for global atmospheric Research. *Scientific Data*, *7*(1), 121. https://doi.org/10.1038/s41597-020-0462-2

Euskirchen, E. S., Bruhwiler, L. M., Commane, R., Parmentier, F.-J. W., Schädel, C., Schuur, E. A., & Watts, J. (2022). Current knowledge and uncertainties associated with the Arctic greenhouse gas budget. In *Balancing greenhouse gas budgets* (pp. 159–201). Elsevier. https://doi.org/10.1016/B978-0-12-814952-2.00007-1

Ganesan, A. L., Rigby, M., Zammit-Mangion, A., Manning, A. J., Prinn, R. G., Fraser, P. J., et al. (2014). Characterization of uncertainties in atmospheric trace gas inversions using hierarchical Bayesian methods. *Atmospheric Chemistry and Physics*, *14*(8), 3855–3864. https://doi.org/10.5194/acp-14-3855-2014

Göckede, M., Reum, F., & Heimann, M. (2023). Atmospheric mixing ratios of CO2 and CH4 at Ambarchik, NE Siberia, 2014-2017 [Dataset]. https://doi.org/10.17617/3.1STIJV

Hatakka, J., & ICOS, R. I. (2022). ICOS atmosphere level 2 data, Pallas, release 2022-1 [Dataset]. *ICOS ERIC—Carbon Portal*. Retrieved from https://meta.icos-cp.eu/collections/6NpfwCWt7VJxybU-USxxpUmC

Hinkel, K. M., Paetzold, F., Nelson, F. E., & Bockheim, J. G. (2001). Patterns of soil temperature and moisture in the active layer and upper permafrost at Barrow, Alaska: 1993–1999. *Global and Planetary Change*, *29*(3), 293–309. https://doi.org/10.1016/S0921-8181(01)00096-0

Hugelius, G., Bockheim, J. G., Camill, P., Elberling, B., Grosse, G., Harden, J. W., et al. (2013). A new data set for estimating organic carbon storage to 3 m depth in soils of the northern circumpolar permafrost region. *Earth System Science Data*, *5*(2), 393–402. https://doi.org/10.5194/essd-5-393-2013

Hugelius, G., Strauss, J., Zubrzycki, S., Harden, J. W., Schuur, E. a. G., Ping, C.-L., et al. (2014). Estimated stocks of circumpolar permafrost carbon with quantified uncertainty ranges and identified data gaps. *Biogeosciences*, *11*(23), 6573–6593. https://doi.org/10.5194/bg-11-6573-2014

Inness, A., Ades, M., Agustí-Panareda, A., Barré, J., Benedictow, A., Blechschmidt, A.-M., et al. (2019). The CAMS reanalysis of atmospheric composition. *Atmospheric Chemistry and Physics*, *19*(6), 3515–3556. https://doi.org/10.5194/acp-19-3515-2019

Ishizawa, M., Chan, D., Worthy, D., Chan, E., Vogel, F., & Maksyutov, S. (2019). Analysis of atmospheric CH4 in Canadian Arctic and estimation of the regional CH4 fluxes. *Atmospheric Chemistry and Physics*, *19*(7), 4637–4658. https://doi.org/10.5194/acp-19-4637-2019

Ivakov, V., Laurila, T., Dlugokencky, E., & Hatakka, J. (2019). Atmospheric CH4 at Tiksi by Finnish Meteorological Institute, dataset published as CH4_tik_surface-insitu_fmi_data1 at WDCGG, ver. 2022-07-08-2150 [Dataset]. *World Data Centre for Greenhouse Gases*. https://doi.org/10.50849/WDCGG_0025-2002-1002-01-01-9999

Jensen, K., & Mcdonald, K. (2019). Surface water Microwave product series version 3: A near-real time and 25-year historical global inundated area fraction time series from active and passive microwave remote sensing. *IEEE Geoscience and Remote Sensing Letters*, *16*(9), 1402–1406. https://doi.org/10.1109/LGRS.2019.2898779

Jones, A., Thomson, D., Hort, M., & Devenish, B. (2007). The U.K. Met Office's next-generation atmospheric dispersion model, NAME III. In C. Borrego & A.-L. Norman (Eds.), *Air pollution modeling and its application XVII* (pp. 580–589). Springer US.

Kittler, F., Heimann, M., Kolle, O., Zimov, N., Zimov, S., & Göckede, M. (2017). Long-term drainage reduces CO 2 uptake and CH 4 emissions in a siberian permafrost ecosystem: Drainage impact on arctic carbon cycle. *Global Biogeochemical Cycles*, *31*(12), 1704–1717. https://doi.org/10.1002/2017GB005774

Lan, X., Dlugokencky, E. J., Mund, J. W., Crotwell, E., Moglia, E., Madronich, M., et al. (2022). Atmospheric methane dry air mole fractions from the NOAA GML carbon cycle cooperative global air sampling network, 1983-2021. https://doi.org/10.15138/VNCZ-M766

Laurila, T. (2023). Data on atmospheric concentrations of CH4, CO and meteorological parameters at Baranova site, Russia [Dataset]. *Finnish Meteorological Institute*. https://fmi.b2share.csc.fi/records/cd485d0c767d47d6b0028c73620eca38

Laurila, T., Asmi, E., Hatakka, J., Kilkki, J., Rainne, J., Mäkelä, T., et al. (2017). On the recent increase of atmospheric methane concentrations as observed at three arctic stations: Tiksi, Pallas, and Ice Base "Cape Baranova". In *Proceedings of the 3rd pan- Eurasian experiment (PEEX) conference and the 7th PEEX meeting*. In *Report Series in Aerosol Science* (Vol. 201, pp. 247–250).

Lehner, B., & Döll, P. (2004). Development and validation of a global database of lakes, reservoirs and wetlands. *Journal of Hydrology*, *296*(1), 1–22. https://doi.org/10.1016/j.jhydrol.2004.03.028

Lunt, M., Manning, A., Allen, G., Arnold, T., Bauguitte, S., Boesch, H., et al. (2021). Atmospheric observations consistent with reported decline in the UK's methane emissions, 2013-2020. *Atmospheric Chemistry and Physics Discussions*, 1–30. https://doi.org/10.5194/acp-2021-548

Mastepanov, M., Sigsgaard, C., Dlugokencky, E. J., Houweling, S., Ström, L., Tamstorf, M. P., & Christensen, T. R. (2008). Large tundra methane burst during onset of freezing. *Nature*, *456*(7222), 628–630. https://doi.org/10.1038/nature07464

Mastepanov, M., Sigsgaard, C., Tagesson, T., Ström, L., Tamstorf, M. P., Lund, M., & Christensen, T. R. (2013). Revisiting factors controlling methane emissions from high-Arctic tundra. *Biogeosciences*, *10*(7), 5139–5158. https://doi.org/10.5194/bg-10-5139-2013

Meredith, M., Sommerkorn, M., Cassotta, S., Derksen, C., Ekaykin, A., Hollowed, A., et al. (2019). Polar Regions. In *IPCC special report on the ocean and cryosphere in a changing climate*.

Miller, S. M., Miller, C. E., Commane, R., Chang, R. Y.-W., Dinardo, S. J., Henderson, J. M., et al. (2016). A multiyear estimate of methane fluxes in Alaska from CARVE atmospheric observations. *Global Biogeochemical Cycles*, *30*(10), 1441–1453. https://doi.org/10.1002/2016GB005419

Morimoto, S., Fujita, R., Aoki, S., Goto, D., & Nakazawa, T. (2017). Long-term variations of the mole fraction and carbon isotope ratio of atmospheric methane observed at Ny-Ålesund, Svalbard from 1996 to 2013. *Tellus B: Chemical and Physical Meteorology*, *69*(1), 1380497. https://doi.org/10.1080/16000889.2017.1380497

Morimoto, S., & Goto, D. (2019). CH4 concentrations observed at Ny-Alesund, Svalbard [Dataset]. *Tohoku University and National Institute of Polar Research*. Retrieved from https://polaris.nipr.ac.jp/~parc/pub/v041/nipr_parc_122_0004.txt

Myhre, G., Shindell, D., Bréon, F.-M., Collins, W., Fuglestvedt, J., Huang, J., et al. (2013). Anthropogenic and natural radiative forcing. In *Climate change 2013: The physical science basis. Contribution of working group I to the fifth assessment report of the intergovernmental panel on climate change*. Cambridge University Press.

Olefeldt, D., Hovemyr, M., Kuhn, M. A., Bastviken, D., Bohn, T. J., Connolly, J., et al. (2021). The boreal-arctic wetland and lake dataset (BAWLD). *Earth System Science Data Discussions*, 1–40. https://doi.org/10.5194/essd-2021-140

Randerson, J., van der Werf, G., Giglio, L., Collatz, G., & Kasibhatla, P. (2017). *Global fire emissions Database, version 4.1 (GFEDv4)*. ORNL Distributed Active Archive Center. https://doi.org/10.3334/ORNLDAAC/1293

Rantanen, M., Karpechko, A. Y., Lipponen, A., Nordling, K., Hyvärinen, O., Ruosteenoja, K., et al. (2022). The Arctic has warmed nearly four times faster than the globe since 1979. *Communications Earth & Environment*, *3*(1), 1–10. https://doi.org/10.1038/s43247-022-00498-3

Rautiainen, K., Parkkinen, T., Lemmetyinen, J., Schwank, M., Wiesmann, A., Ikonen, J., et al. (2016). SMOS prototype algorithm for detecting autumn soil freezing. *Remote Sensing of Environment*, *180*, 346–360. https://doi.org/10.1016/j.rse.2016.01.012

Reum, F., Göckede, M., Lavric, J. V., Kolle, O., Zimov, S., Zimov, N., et al. (2019). Accurate measurements of atmospheric carbon dioxide and methane mole fractions at the Siberian coastal site Ambarchik. *Atmospheric Measurement Techniques*, *12*(11), 5717–5740. https://doi.org/10.5194/amt-12-5717-2019

Rößger, N., Sachs, T., Wille, C., Boike, J., & Kutzbach, L. (2022). Seasonal increase of methane emissions linked to warming in Siberian tundra. *Nature Climate Change*, *12*(11), 1031–1036. https://doi.org/10.1038/s41558-022-01512-4

Sasakawa, M. (2023a). Semi-continuous observational data for atmospheric CO2 and CH4 mixing ratios at Azovo, ver1.0 [Dataset]. *Earth System Division, NIES*. Retrieved from https://www.nies.go.jp/doi/10.17595/20231117.007-e.html

Sasakawa, M. (2023b). Semi-continuous observational data for atmospheric CO2 and CH4 mixing ratios at Berezorechka, ver1.0 [Dataset]. *Earth System Division, NIES*. Retrieved from https://www.nies.go.jp/doi/10.17595/20231117.001-e.html

Sasakawa, M. (2023c). Semi-continuous observational data for atmospheric CO2 and CH4 mixing ratios at Karasevoe, ver1.0 [Dataset]. *Earth System Division, NIES*. Retrieved from https://www.nies.go.jp/doi/10.17595/20231117.002-e.html

Sasakawa, M. (2023d). Semi-continuous observational data for atmospheric CO2 and CH4 mixing ratios at Noyabrsk, ver1.0 [Dataset]. *Earth System Division, NIES*. Retrieved from https://www.nies.go.jp/doi/10.17595/20231117.004-e.html

Sasakawa, M. (2023e). Semi-continuous observational data for atmospheric CO2 and CH4 mixing ratios at Vaganovo, ver1.0 [Dataset]. *Earth System Division, NIES*. Retrieved from https://www.nies.go.jp/doi/10.17595/20231117.008-e.html

Sasakawa, M., Shimoyama, K., Machida, T., Tsuda, N., Suto, H., Arshinov, M., et al. (2010). Continuous measurements of methane from a tower network over Siberia. *Tellus B: Chemical and Physical Meteorology*, *62*(5), 403. https://doi.org/10.3402/tellusb.v62i5.16583

Saunois, M., Stavert, A. R., Poulter, B., Bousquet, P., Canadell, J. G., Jackson, R. B., et al. (2020). The global methane budget 2000–2017. *Earth System Science Data*, *12*(3), 1561–1623. https://doi.org/10.5194/essd-12-1561-2020

Say, D., Kuyper, B., Western, L., Khan, M. A. H., Lesch, T., Labuschagne, C., et al. (2020). Emissions and marine boundary layer concentrations of unregulated chlorocarbons measured at Cape point, South Africa. *Environmental Science and Technology*, *54*(17), 10514–10523. https://doi.org/10.1021/acs.est.0c02057

Schuldt, K. N., Mund, J., Aalto, T., Andrews, A., Apadula, F., Arduini, J., et al. (2023). Multi-laboratory compilation of atmospheric carbon dioxide data for the period 1983-2022; obspack_ch4_1_globalviewplus_v6.0_2023-12-01 [Dataset]. *NOAA Global Monitoring Laboratory*. Retrieved from https://gml.noaa.gov/ccgg/obspack/data.php?id=obspack_ch4_1_GLOBALVIEWplus_v6.0_2023-12-01

Sweeney, C., Dlugokencky, E., Miller, C. E., Wofsy, S., Karion, A., Dinardo, S., et al. (2016). No significant increase in long-term CH4 emissions on North Slope of Alaska despite significant increase in air temperature. *Geophysical Research Letters*, *43*(12), 6604–6611. https://doi.org/10.1002/2016GL069292

Tao, J., Zhu, Q., Riley, W. J., & Neumann, R. B. (2021). Improved ELMv1-ECA simulations of zero-curtain periods and cold-season CH4 and CO2 emissions at Alaskan Arctic tundra sites. *The Cryosphere*, *15*(12), 5281–5307. https://doi.org/10.5194/tc-15-5281-2021

Tenkanen, M., Tsuruta, A., Rautiainen, K., Kangasaho, V., Ellul, R., & Aalto, T. (2021). Utilizing earth observations of soil freeze/thaw data and atmospheric concentrations to estimate cold season methane emissions in the northern high latitudes. *Remote Sensing*, *13*(24), 5059. https://doi.org/10.3390/rs13245059

Thompson, R. L., Sasakawa, M., Machida, T., Aalto, T., Worthy, D., Lavric, J. V., et al. (2017). Methane fluxes in the high northern latitudes for 2005–2013 estimated using a Bayesian atmospheric inversion. *Atmospheric Chemistry and Physics*, *17*(5), 3553–3572. https://doi.org/10.5194/acp-17-3553-2017

Thoning, K. W., Tans, P. P., & Komhyr, W. D. (1989). Atmospheric carbon dioxide at Mauna Loa observatory: 2. Analysis of the NOAA GMCC data, 1974–1985. *Journal of Geophysical Research*, *94*(D6), 8549–8565. https://doi.org/10.1029/JD094iD06p08549

Thornton, B. F., Wik, M., & Crill, P. M. (2016). Double-counting challenges the accuracy of high-latitude methane inventories. *Geophysical Research Letters*, *43*(24), 12569–12577. https://doi.org/10.1002/2016GL071772

Treat, C. C., Bloom, A. A., & Marushchak, M. E. (2018). Nongrowing season methane emissions–a significant component of annual emissions across northern ecosystems. *Global Change Biology*, *24*(8), 3331–3343. https://doi.org/10.1111/gcb.14137

Tsuruta, A., Kivimäki, E., Lindqvist, H., Karppinen, T., Backman, L., Hakkarainen, J., et al. (2023). CH4 fluxes derived from assimilation of TROPOMI XCH4 in CarbonTracker Europe-CH4: Evaluation of seasonality and spatial distribution in the northern high latitudes. *Remote Sensing*, *15*(6), 1620. https://doi.org/10.3390/rs15061620

Tunnicliffe, R. L., Ganesan, A. L., Parker, R. J., Boesch, H., Gedney, N., Poulter, B., et al. (2020). Quantifying sources of Brazil's CH4 emissions between 2010 and 2018 from satellite data. *Atmospheric Chemistry and Physics Discussions*, 1–40. https://doi.org/10.5194/acp-2020-438

Turetsky, M. R., Abbott, B. W., Jones, M. C., Walter Anthony, K., Olefeldt, D., Schuur, E. A. G., et al. (2019). Permafrost collapse is accelerating carbon release. *Nature*, *569*(7754), 32–34. https://doi.org/10.1038/d41586-019-01313-4

Ward, R. H. (2024a). CH4 top-down emissions from three high-latitude Arctic regions [Dataset]. *Zenodo*. https://doi.org/10.5281/ZENODO.10782557

Ward, R. H. (2024b). Wind sector analysis of CH4 observations at Barrow, Alaska. *Zenodo*. https://doi.org/10.5281/zenodo.10814752

Weber, T., Wiseman, N. A., & Kock, A. (2019). Global ocean methane emissions dominated by shallow coastal waters. *Nature Communications*, *10*(1), 4584. https://doi.org/10.1038/s41467-019-12541-7

Wilkman, E., Zona, D., Tang, Y., Gioli, B., Lipson, D. A., & Oechel, W. (2018). Temperature response of respiration across the heterogeneous landscape of the Alaskan arctic tundra. *Journal of Geophysical Research: Biogeosciences*, *123*(7), 2287–2302. https://doi.org/10.1029/2017JG004227

Wittig, S., Berchet, A., Pison, I., Saunois, M., Thanwerdas, J., Martinez, A., et al. (2023). Estimating Methane Emissions in the Arctic nations using surface observations from 2008 to 2019 [preprint]. *Atmospheric Chemistry and Physics*, *23*(11), 6457–6485. https://doi.org/10.5194/acp-23-6457-2023

Xu, X., Yuan, F., Hanson, P. J., Wullschleger, S. D., Thornton, P. E., Riley, W. J., et al. (2016). Reviews and syntheses: Four decades of modeling methane cycling in terrestrial ecosystems. *Biogeosciences*, *13*(12), 3735–3755. https://doi.org/10.5194/bg-13-3735-2016

Zhang, Z., Fluet-Chouinard, E., Jensen, K., McDonald, K., Hugelius, G., Gumbricht, T., et al. (2020). Development of a global dataset of wetland area and dynamics for methane modeling (WAD2M). *Earth System Science Data Discussions*, 1–50. https://doi.org/10.5194/essd-2020-262

Zona, D., Gioli, B., Commane, R., Lindaas, J., Wofsy, S. C., Miller, C. E., et al. (2016). Cold season emissions dominate the Arctic tundra methane budget. *Proceedings of the National Academy of Sciences*, *113*(1), 40–45. https://doi.org/10.1073/pnas.1516017113